Pol. J. Environ. Stud. Vol. 31, No. 4 (2022), 3611-3626
DOI: *10.15244/pjoes/146937* ONLINE PUBLICATION DATE: 2022-05-17

Original Research

Characterizing the Fundamental Controls on Deformation and Stability of an Active Reservoir Landslide, Southwest China

Muhammad Kamran[1]*, Xiewen Hu[1], Muhammad Awais Hussain[2], Kun He[1], Adil Nawaz[3], Randa Ali[1]

[1]Faculty of Geosciences and Environmental Engineering, Southwest Jiaotong University, Chengdu, 611756, China
[2]College of Civil Engineering and Architecture, Zhejiang University, Hangzhou, China
[3]Faculty of Geology Geophysics and Environmental Protection AGH University of Science and Technology, Krakow 30-059, Poland

Received: 11 October 2021
Accepted: 24 February 2022

Abstract

After the normal operation of the Qiaoqi reservoir in 2007, about 40 landslides have been triggered by the influence of reservoir levels and precipitation, that caused a serious threat to socio-economic activities. Taking the Kadui-2 landslide as a case study, three-year (2015-2017) GPS monitoring network was implemented to observe surface deformation. Based on the reservoir level fluctuation and precipitation, coupled seepage-stability simulations were conducted using Geo-studio to obtain distribution behavior of saturation lines and stability. The slide mass experienced persistent deformation with a maximum cumulative displacement of 331.34 cm. The long-term displacement data shows a step-like characteristic and follows an acceleration phase from December to April during reservoir draw-down periods and subsequent low strain rate from May to November during reservoir-filling operation. The simulation results reveal that the landslide stability lag behind the reservoir level and maximum internal hydraulic forces are operating within the saturation zone. The landslide stability and displacement rate is dominantly controlled by the change of reservoir level only and rainfall has no significant effect. Furthermore, the total collapsed area increased significantly by 18 % from 2012 to 2014 at the head of landslide that shows a retrogressive type movement.

Keywords: reservoir landslide, reservoir level fluctuation; rainfall, cumulative displacement, deformation characteristics

Introduction

Reservoir landslides are a common type of geological disasters in hydropower surroundings, which cause a severe socio-economic threat to human life [1]. Generally, narrow and steep valleys are prone to landslides [2-4]. Wavefront slopes in reservoir reservoir project area are greatly affected by water level changes and may fail easily [5-7]. For example, the catastrophic Vajont landslide in Italy 1963 and the Qianjianping landslide of China in 2003, both disaster events triggered by the variation of reservoir level [8-9].

*e-mail: mkamran@my.swjtu.edu.cn

Landslides in Three Gorges reservoir are distributed into three categories based on the mechanism of landslide instability [10], most of sliding mass are hydrodynamic landslides triggered by water level fluctuation [11]. The reservoir impoundment has significantly altered the original geological conditions and enlarge the frequency of natural disasters, especially landslides [12]. The fluctuation zone undergoes wetting-drying cycles which will lead to deteriorating the slide mass and the sliding belt reflect the prime control over deformation and stability of landslide [13]. The stability and deformation behavior of a reservoir landslide is governed by external water loadings, pore pressure and soil properties [14-15]. Due to cyclic changes in water level and precipitation, the slip zone soil undergoes a variation in moisture content and seepage field, which will consequently influence the shear strength of slide mass [16-18]. The Stability of a reservoir slope is primarily controlled by water level changes [19] and very important to the safe operation of highways, infrastructures and the life span of the resevoir [20-23]. A recent study reveals that 90% of slide mass deformations are associated with pore pressure [24]. Particular considerations comprise (1) Load changes are observed in reservoir slopes as a result of indunation when reservoir is filled and subsequently, drawdown operation; (2) Properties of slide mass and bedrock are affected by reservoir hydraulic operation and cause serious consequences; (3) Water level variation increases the chances and consequences of failures, which can cause partial or total blockage of reservoir and the possibility of impulse waves which may have severe effects that can extend beyond the reservoir.

Seasonal rainfall is also a key trigger for landslides, which can penetrate into the slope mass along the cracks, enhance the weight of slide mass and cause landslide deformation [25-29]. Infiltration channels can be produced on reservoir slope along the existing cracks [30-32]. Rainwater can percolate through infiltration channels, reducing strength parameters of soil, consequently increasing failure chances [33-36]. Coupled DEM modeling for Qioaqi landslide revealed that the reservoir level and precipitation tended to destabilize the lower and upper part of slope [37].

After the normal operation of Qiaoqi hydropower station in 2007, the reservoir follows two-phase of water level variation, every November-April for water supply period and May-October for water impoundment period. During the process of water level variation, road subsidence, damage to houses and dozens of landslide occurred. About 40 distorted slopes of different sizes have been marked in reservoir surrounding (Fig. 1c). The number of landslides, road subsidence and damage to houses continue to increase in the subsequent years, showing that the deformation process responds to hydraulic processes accordingly. The landslide deformation not only causes damage to buildings, cracking highway, subgrades settlements but also has a certain degree of reservoir siltation due to the failure of a large number of slopes in reservoir. The reservoir landslide and consequences have a massive threat for the people living in the reservoir area and the safe operation of the dam [38-41]. Therefore, many residents moved to safe places because of the severe effects of landslides that can cause loss of human life. Based on monitoring data and field surveys, the deformation characteristics and mechanisms of Kadui-2 (KD-2) landslide are investigated in the Qiaoqi reservoir. According to the reservoir running curve and precipitation, simulation for the seepage field and stability coefficient is conducted using a numerical model. The findings allow to define the variation of slope stability and deformation behavior under varying conditions.

Background

Study Area and Landslide Features

Baoxing county is located in the southwestern segment of the Longmenshan Fault zone and overlaid by the Baoxing Massif which primarily consists of Precambrian rocks [42-43]. The Kadui-2 landslide occurred about 4.5 km upstream on the right bank of Qiaoqi reservoir, Baoxing county, Yaan [44]. Deep cut river valleys and steep mountains of high altitudes are the main geomorphic characteristics of this area. The typical altitude of surrounding mountains is more than 2500 m above sea level and the flow of the Baoxing river near the dam site is from North to South. The study area falls in the sub-tropical zone with mean temperature -1.1ºC in January, 18.1ºC in July and an annual mean temperature of 8.8ºC. The Baoxing river having an average gradient of 24.2% is rich for hydropower stations and mainly recharged by precipitation. The KD-2 landslide ranges from 2050 m to 2250 m in elevation, 547.96 m width and a maximum longitudinal length of 530 m along the river.

Based on deformation characteristics and configuration, the Kadui-2 landslide is divided into three main parts KD2-1, KD2-2, and KD2-3 respectively. KD2-1 is the eastern marginally part, KD2-2 longitudinally elongated central part and KD2-3 constitutes the largest part lies in the western side of the landslide (Fig. 2). The marginal parts are elongated than the central part and the terrain slope trend is 15°~35° for all parts. The collapsed range measured by the end of 2012 is represented by gray line and after this a sharp edge extended out from KD2-1 and KD2-3 with a total increase of 13450 m^2 area in the extended range compared to 2012, increased by 18.7 % accordingly until 2104 (Fig. 2).

A detailed field survey was conducted in Kadui-2 landslide territory to observe slide mass activity features. Numerous surficial tension cracks 7-18 cm deep, 6-15 cm wide, up to 10-30 cm length were observed at the leading edge, while the length of shear cracks at the edge boundaries range from 10~32 m.

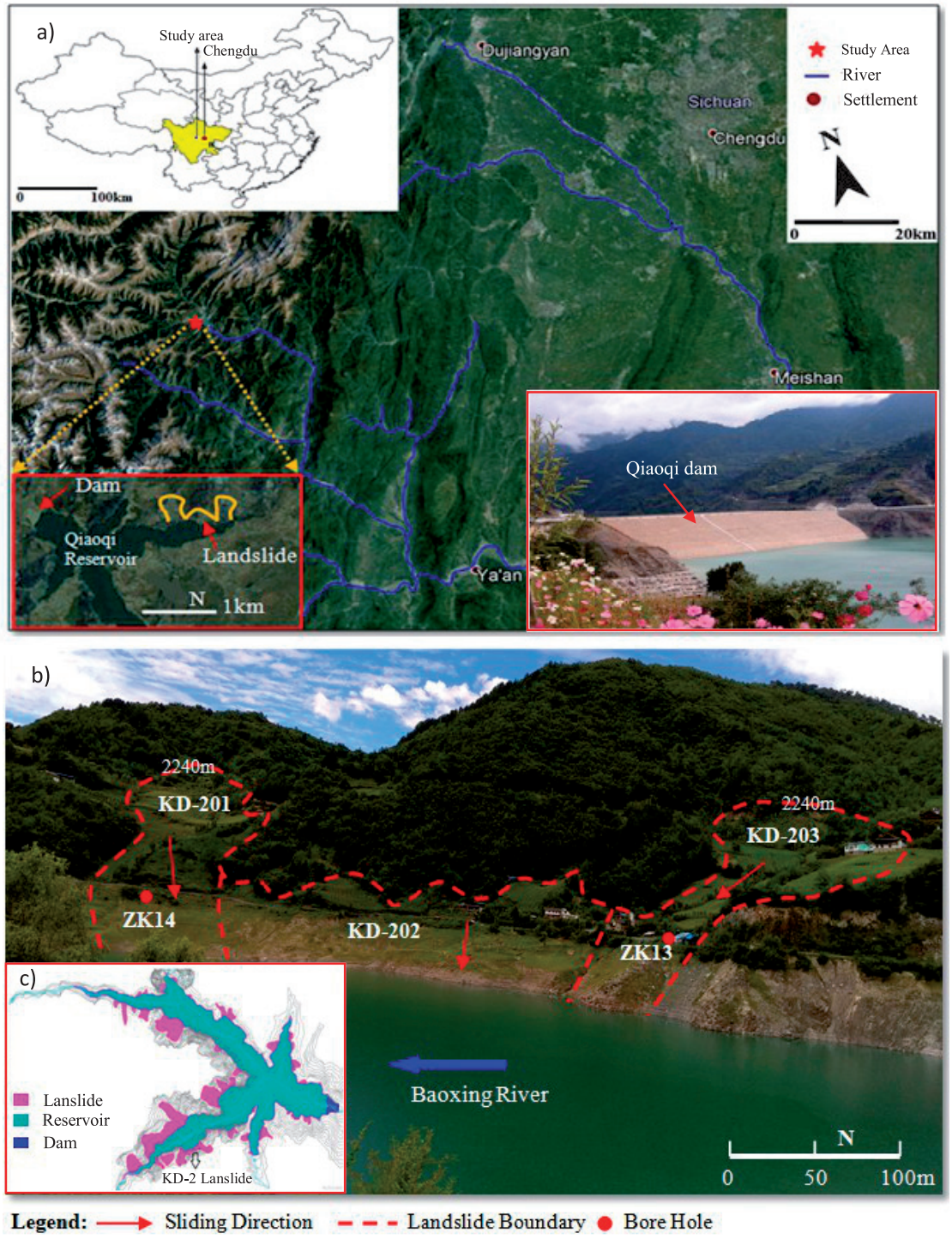

Fig. 1. a) Location map of the study area; b) An overview of landslide; c) Landslides distribution in reservoir surrounding.

Additionally, the new cracks have been developed during the repeated reservoir filling-drawdown cycles. Two large trenches located at the side boundaries of KD-2 landslide cause crack development and accelerate the movement rate (Fig. 2a). In the Kd2-2 slide mass, a stepwise scarp 0.4 m was found (Fig. 2f). Long-lasting creep behavior of landslide can be observed by bending tress (Fig. 2d). The deformation of surficial mass subsidized the road about 2.5 m along the reservoir annually (Fig. 2e). Under the influence of creeping, large shear cracks were observed on the retaining structures (Table 1). These forementioned landslide activity features indicate that Kadui-2 landslide progressively moves with localized creep deformations. Maximum displacement 32.3 cm was observed at KD2-1 slide mass after first impoundment and after that reservoir seasonal fluctuation enhances the deformation grade. Left marginal part KD2-3 shows little deformation rate with an average displacement of 2.5 cm/year. Softening and draining action of running water from the slope

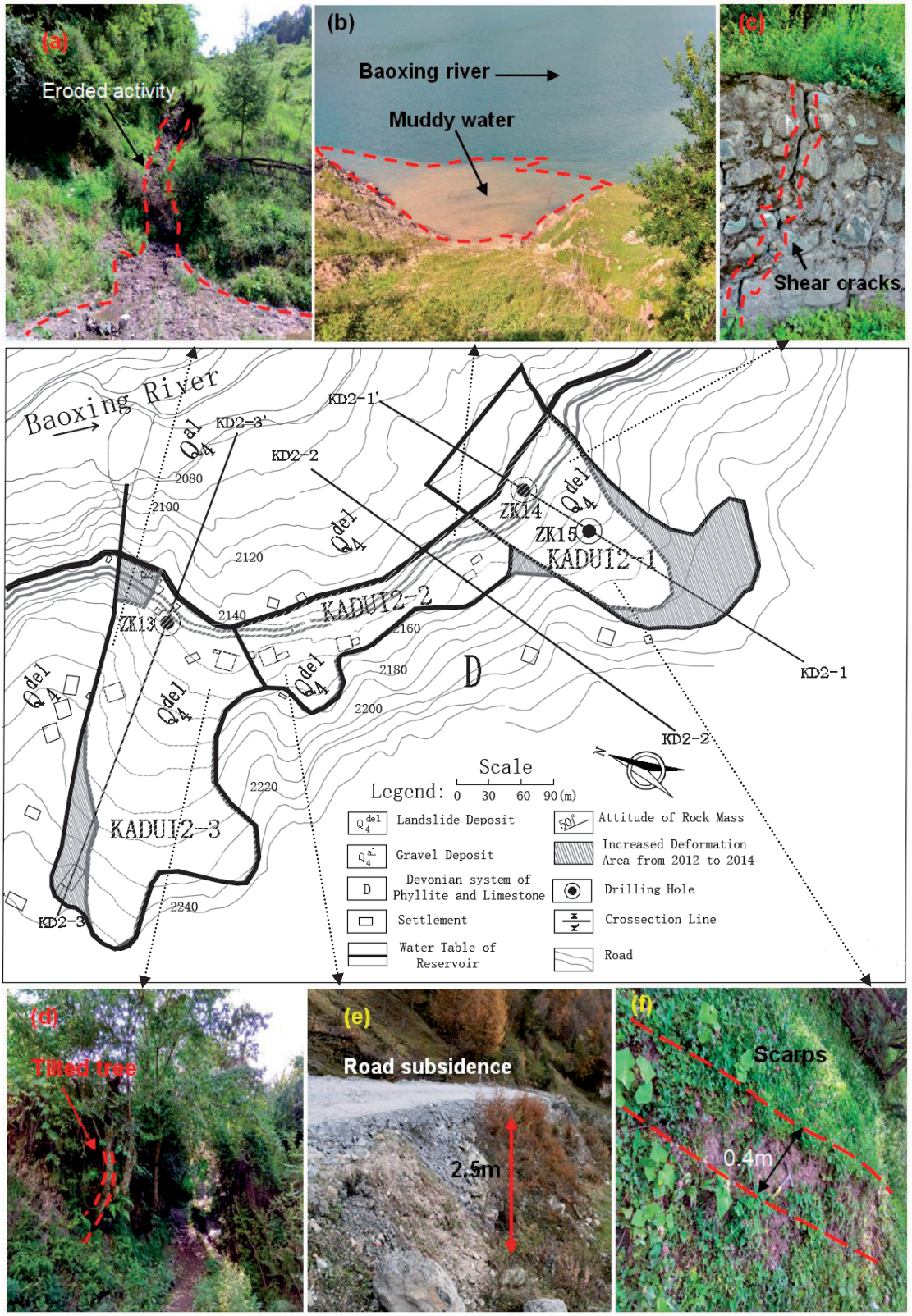

Fig. 2. a) Eroded activity; b) Reservoir mingling with sediment; c) Cracks on retaining wall; d) Creeping; e) Road subsidence; f) Scarp.

mass is termed as erosion [45-46]. Field study shows that the sediment erosion by running water is widely distributed in reservoir surrounding and accelerates the deformation rate. As described, the flabbiness layer of slide mass consists of mainly sandy-silty-clayey gravel that can be eroded easily by dynamic running water. Thus, muddy water emerging from slide mass can be observed at the toe of the slope and resulting eroded trenches occur at the side boundaries of slide mass (Fig. 2b).

Table 1. The Cracks observed on Kadui-2 Landslide.

Cracks	Trend (^{0})	Length (m)	Width (cm)	Depth (cm)	Mechanism
LF1	72	28	10	15	Shear
LF2	17	10	5	3	Tension
LF3	166	21	7	6	Tension
LF4	30	22	5	7	Tension
LF5	175	23	15	16	Tension
LF6	106	22	8	10	Shear
LF7	46	35	15	18	Tension
LF8	112	28	10	11	Tension
LF9	141	14	6	8	Tension
LF10	154	27	11	9	Tension
LF11	113	22.5	12	8	Tension
LF12	29	24	8	6	Shear

Composition

Lithology of the landslide area mainly consists of Quarternary (Q_4^{del}) deposit and is underlain by Devonian (D) bedrocks. Poorly graded Quarternary slide mass consists of alluvial gravel and reddish-brown sandy-silty-clayey particles. Glacial deposit gravels are characterized by angular-subangular and a few subround gravel. Bedrock is composed of the Devonian system (D) greyish black carbonaceous Silty Phyllite layers of thickness less than 1 cm. The grain size distribution of the slide mass soil is 16.37 % clay, 11.99 % silt, 5.73 % fine sand and 65.9 % gravelly soil. At the toe of landslide, a thick layer of alluvial gravel (Q_4^{al}) deposited.

Method

Field Monitoring

A series of five GPS monitoring stations, A-1, A-2, B-1, B-2, and C-1 are deployed in the Kadui-2 landslide area to monitor surface displacement (Horizontal, Vertical) from the period, December 2014 to July 2017 (Fig. 4b). Monitoring results indicate that accumulated displacements for A-1, A-2 and B-2 are fast, having stepwise characteristics, while B-1 and C-1 show steady slow displacement increment. Generally, horizontal displacement is greater than the associated vertical displacement because of the small dip slope angle.

Numerical Modeling and Operating Scheme

A Two-dimensional finite element SEEP/W and SLOPE/W modules of Geostudio suite (version 8.15 Geoslope international Ltd 2012) were used to perform coupled seepage-stability analysis of landslide. The geomechanical model mainly comprises two different layers, Silty sandy clay with fragmented gravels in the slide part and Silty Phyllite as bedrock. The silty sandy clay and fragmented cobbles are shown by light yellow and Silty Phyllite by light green color (Fig. 6). The physio-mechanical parameters of Kadui-2 landslide are determined (Table 2) based on laboratory experiments and geological prospecting.

Transient seepage analysis based on the actual reservoir level and rainfall is carried out by using SEEP/W under saturated-unsaturated material mode. Saturated and Saturated-Unsaturated are commonly used material mode in SEEP/W for seepage analysis. The saturated model is useful for steady state analysis on a region that always remains below the water level, while the saturated-unsaturated model is applicable for slope mass if unsaturated zones are expected to occur. In the Kadui-2 landslide, reservoir level fluctuates

Table 2. Parameters for stability calculation.

	Natural State			Saturation State		
	Unit Weight	Cohesion	Internal Friction angle	Unit Weight	Cohesion	Internal Friction angle
	(kN/m^3)	(kPa)	(°)	(kN/m^3)	(kPa)	(°)
Sliding body	19.7	30	17	21	10	30

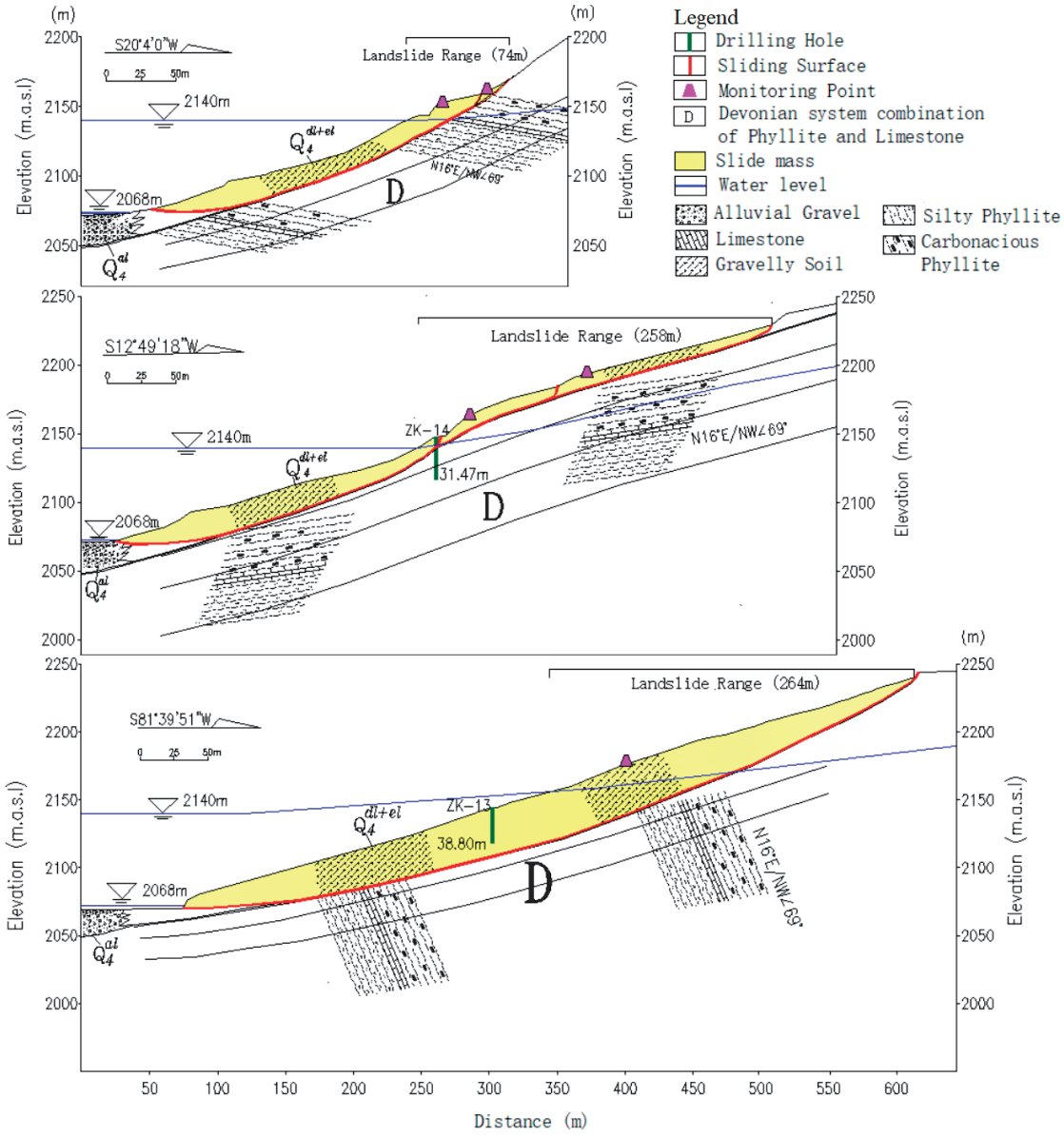

Fig. 3. Cross sections of KD-2 landslide.

from 2068 m to 2140 m, which reveals the existence of partially saturated zones. So, saturated-unsaturated material mode is adopted for transient state seepage analysis of Kadui-2 landslide. In saturated-unsaturated model, a function for volumetric water content and hydraulic conductivity should be provided. Volumetric water content function is used for estimation of hydraulic conductivity function. So, it is necessary to develop a volumetric water content function to determine hydraulic conductivity function.

Then pore water pressure results were used in limit equilibrium SLOPE/W model using the Morgenstern-Price method to find out stability coefficient. Seepage partial differential equation requires various soil hydraulic functions as follows:

$$\frac{\partial}{\partial x}\left(Kx\frac{\partial H}{\partial x}\right) + \partial/\partial y\,(Ky\frac{\partial H}{\partial y}) + Q = \partial\theta/\partial t \quad (1)$$

Where Kx and Ky are hydraulic conductivity in x, y direction respectively, H is the total hydraulic head, Θ is the volumetric water content, Q is the applied boundary flux, and t is the time. Under normal operating conditions, the reservoir level fluctuates between 2168 m and 2140 m (Fig. 4). As the head boundary of landslide varies as reservoir level, so the designed function of water head is as follows:

$$H(t) = \begin{cases} 0.4t, t\ \varepsilon\ (0,180\text{d}) \\ 0.8t, t\ \varepsilon\ (0,90\text{d}) \\ 1.2t, t\ \varepsilon\ (0,60\text{d}) \end{cases} \quad (2)$$

The transient state seepage analysis and stability factor is determined under the coupled operating conditions of reservoir level and rainfall for a complete cycle (Table 3). The increasing rate of water level from 2068 m to 2140 m, are set to as Vr1 = 0.4 m/day,

Fig. 4. Field monitoring a) Double-Ring Permeability test; b) Monitoring station.

Vr2 = 0.8 m/day and Vr3 = 1.2 m/day and the corresponding time periods are 180 days, 90 days and 60 days respectively. The rate of decrease of reservoir level are defined as Vd1 = 0.4 m/day, Vd2 = 0.8 m/day and Vd3 = 1.2 m/day accordingly. At different reservoir fluctuation rates, Vr1, Vr2, Vr3, Vd1, Vd2, and Vd3, the average precipitation distributed accordingly (Table 3). The boundary conditions were set as; Reservoir water level fluctuation determine the boundary condition in the frontal part of landslide, while at the backside constant head boundary condition applied as no change in water level. The sliding surface is an impermeable boundary, Rainfall infiltration boundary applied above the surface of the reservoir level. Reservoir water level range 2068 m-2140 m as variable water head and the height of the initial water head is set as 2140 m.

Results

To examine slope deformation in detail, different operating conditions are employed to determine the seepage behavior and stability of KD2-1 slide mass (Table 3). It registers the seep lines, saturation zone and stability factor.

Transient State Seepage Field Analysis

At different rates of reservoir water level fluctuation, seep lines change accordingly. Fig. 5 shows that seep lines declines during reservoir drawdown. Seep lines are close to each other at a low fluctuation rate and get separated at a high fluctuation rate of reservoir level. The saturation zone occurred just below the maximum reservoir level in all operating conditions. The saturation zone gets thinner as reservoir level drops and has a maximum width at the highest water level. Generally, the groundwater lags behind the reservoir level during fluctuation.

Comparatively, the seep lines are concentrated in a small space during the declining than the rising of the reservoir level. During the drawdown process, the higher groundwater level, large hydraulic gradient and small pore water pressure resulted. According to Darcy's law a large hydraulic gradient would induce larger seepage forces so, maximum seepage occurred during this period resulting in a small seep zone (Fig. 6a). During the rise of reservoir level, the lower groundwater, small hydraulic gradient and high pore water pressure, cause the hydrostatic pressure increment rapidly. As a result, seep lines are widely spaced and concentrated in a large zone (Fig. 6b).

Table 3. Operating conditions for stability calculation.

Number of conditions	Reservoir water level	Fluctuation rate of reservoir water level (m/day)
1.1	Reservoir water level decline from 2140 m to 2068 m	0.4 m/day
1.2		0.8 m/day
1.3		1.2 m/day
2.1	Reservoir water level increase from 2068 m to 2140 m	0.4 m/day
2.2		0.8 m/day
2.3		1.2 m/day

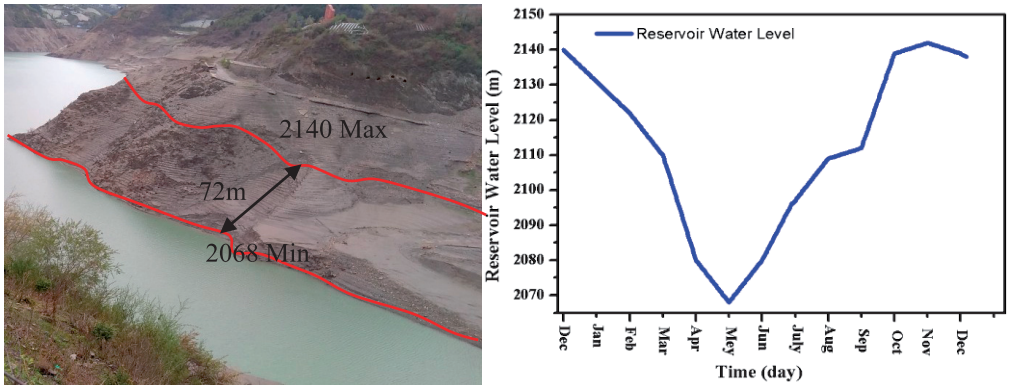

Fig. 5. Annual water level variation.

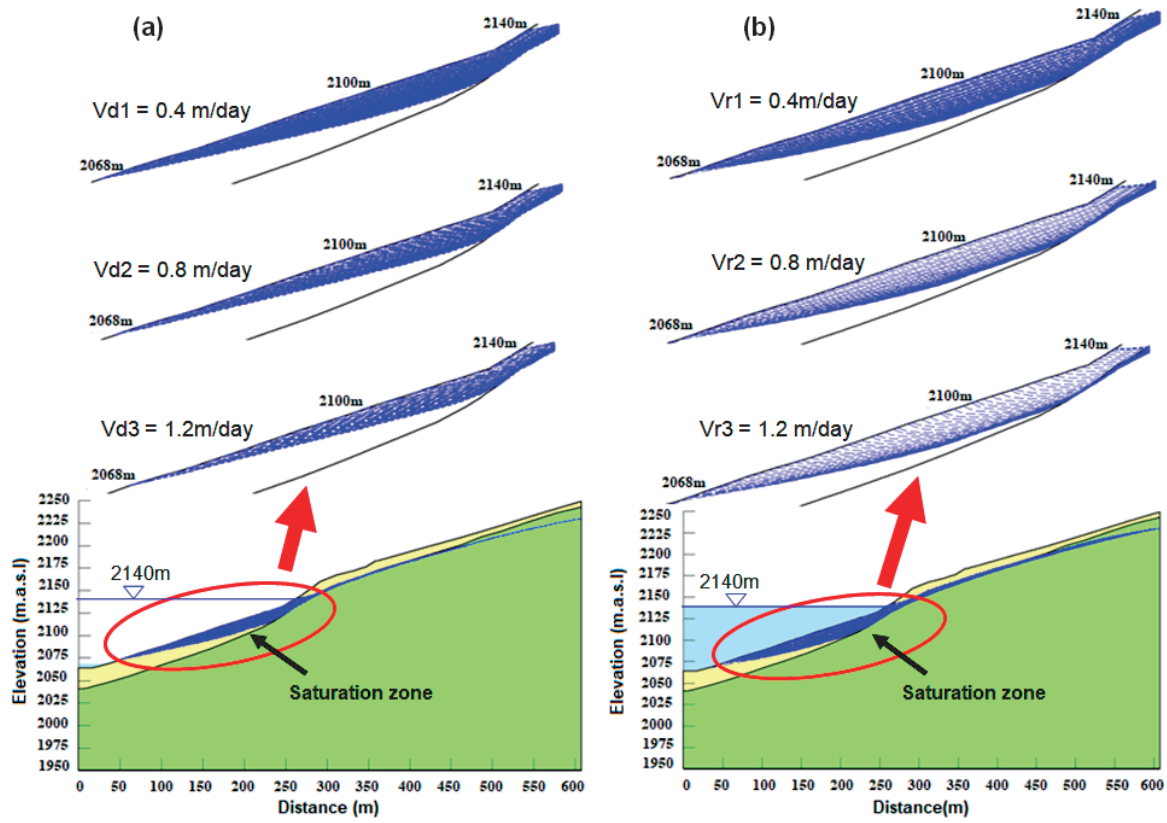

Fig. 6. Seep lines characteristics a) Conditions 1.1, 1.2 and 1.3; b) Conditions 2.1, 2.2, and 2.3.

Stability Coefficient Analysis

The stability coefficient of Kadui-2 landslide is calculated under the periodic variation of reservoir level and precipitation. Since about 50 % of slide mass lies above maximum reservoir level 2140 m, the continuous rainfall seepage will saturate the upper landslide mass and the stability of landslide will further reduce. Rainfall seepage contributes significantly to the slope deformation [47-48]. The relationship between stability coefficient, reservoir level fluctuation, and precipitation shows that the stability coefficient appears to lag behind the reservoir level (Fig. 7a). The stability coefficient decreased upto 10 % only after considering the rainfall. Taking the coupling effects of reservoir level and precipitation, the stability coefficient is less than one calculated by only considering the reservoir level variation (Fig. 7a). Therefore, water level fluctuation is the primary trigger and accumulated rainfall may affect the stability coefficient slightly. The smaller stability coefficient often results during the period of rapid reservoir drawdown and low precipitation (from November to April every year).

The stability coefficients of Kadui-2 landslide are also calculated under different reservoir level rate from 2140 m to 2068 m. Table 4 shows that the

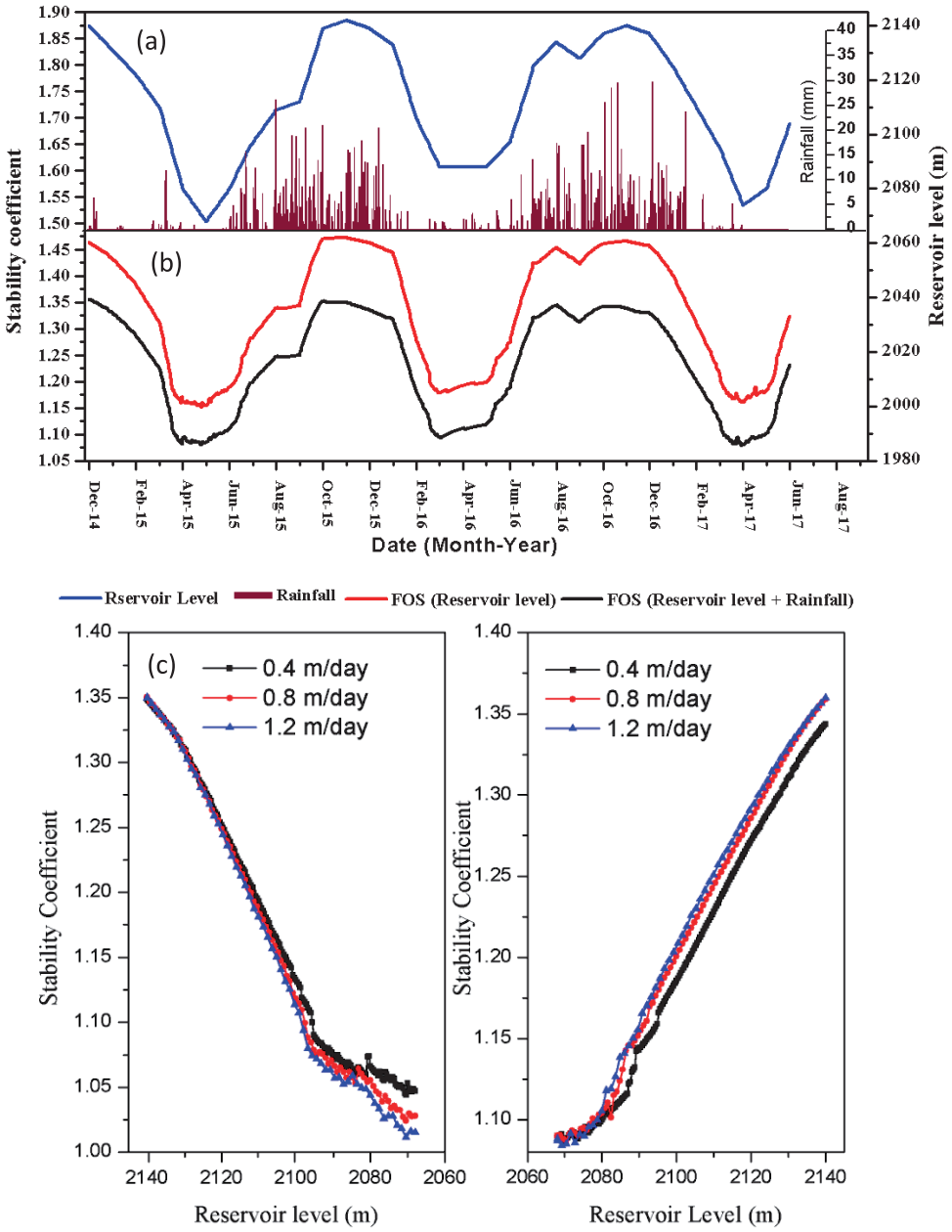

Fig. 7. Stability coefficient evolution under; a) Reservoir level and Precipitation b) Reservoir drawdown; c) Reservoir filling.

maximum stability coefficient is 1.348 at 2140 m when the reservoir rising rate is 0.3 m/day. Moreover, the minimum stability coefficient is 0.952 at 2068 m when the reservoir declining rate is 0.9 m/day. Fig. 7 shows the stability coefficients of Kadui-2 landslide under different operating schemes. Stability coefficients are greatly influenced by reservoir level and exhibit specific characteristics. Fig. 7b) shows that under operating conditions 1.1, 1.2 and 1.3, as the water level declines from 2140 m to 2068 m, the stability coefficient decreases gradually. This is because that the reverse hydrodynamic pressure on the slide mass increases as the reservoir level decreases. The hydrostatic pressure decreases during reservoir drawdown, so a small stability coefficient occurred at high declining rate.

Table 4. Stability coefficient at extreme water levels under different conditions.

Conditions	1.1	1.2	1.3	2.1	2.2	2.3
Water level of 2140 m	1.35	1.35	1.35	1.09	1.09	1.09
Water level of 2068 m	1.05	1.03	1.02	1.34	1.35	1.36

Fig. 7 shows that the stability coefficient lags behind the reservoir level, it increases as the reservoir level rises. This is because that the hydrodynamic pressure and hydrostatic pressure increases when the water level increase. Large hydrostatic pressure is generated at high rate of reservoir level increment, so it causes a large stability coefficient.

Discussion

Slope Deformations vs Reservoir Level Fluctuation and Rainfall

A series of five GPS monitoring stations (A-1, A-2, B-1, B-2 and C-1 selected) randomly were

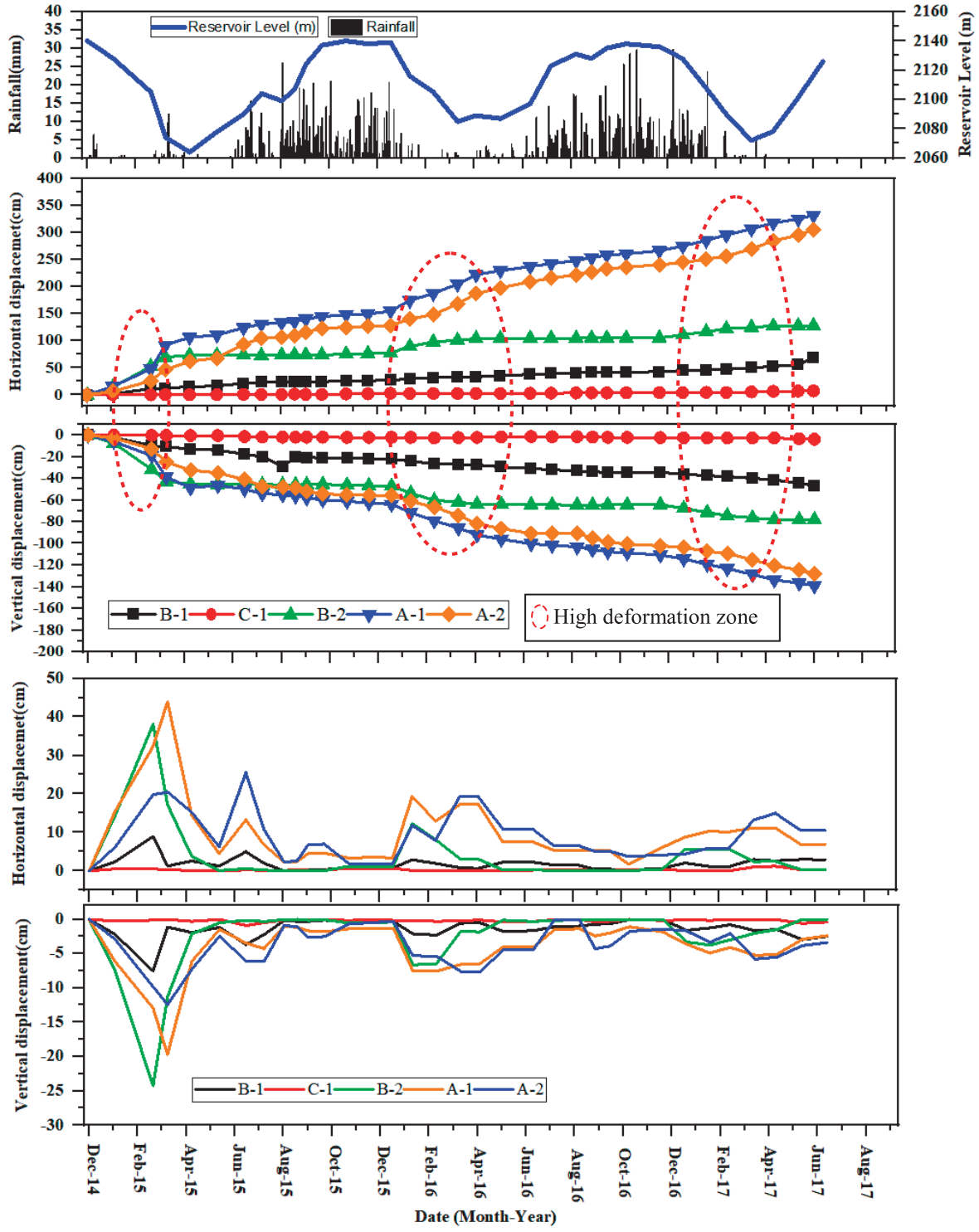

Fig. 8. Relationships between displacement, rainfall and reservoir level; a) Reservoir level and precipitation; b) Cumulative displacement; c) Monthly displacement.

installed to calculate surface deformation continuously from December 2104 to July 2016 (Fig. 8b). KD2-1 and KD2-2 show greater deformation rate than KD2-3, maximum cumulative displacement 333.3 cm is observed at A-1 monitoring station and minimum 7.1 cm at C-1 point. The displacement rate varied spatially, Fig. 8b) shows that the vertical deformation demonstrates essentially the same trend as horizontal. An abrupt increase in displacemet can be observed every December and then slide mass follows a slow and consistent movement (Fig. 8b). The maximum annually cumulative displacement and monthly speed occurred in 2015. Monitoring points on right marginal part KD2-1 shows a high deformation rate than KD2-2 and KD2-3 zone and displacement rate decreases from right marginal part to left marginal zone. The monitored data indicates that several factors are associated with the movement of slide mass, such as reservoir level changes, drawdown velocity and precipitation. In this study, time-dependent deformation of Kadui-2 landslide and related triggering parameters are studied based on the monitoring point.

– A strong seasonal influence on the deformation behavior can be observed in the reservoir drawdown process and a semi-constant slow deformation during filling operation. To analyze each factor in detail, monitored displacements are used to establish a relationship between hydrological triggering factors and slope velocity. Among the GPS measuring stations, the horizontal displacement recorded at point A-1 was maximum and the magnitude reached 331.34 cm till July 2106, of which 208.9 cm occurred during reservoir drawdown from November to April and rest of 122.44 cm in reservoir filling operation from May to October every year. Maximum vertical displacement is also observed at point A-1 with magnitude -138.9 cm, of which -89.144 cm occurred during reservoir declining and remaining -49.756 cm during reservoir impoundment. A similar correlation between reservoir level, precipitation and deformation has been captured by other monitoring stations. At point A-1, A-2 and B-2 displacement time curve also evince step degradation, both for horizontal and vertical displacements. A comparison of cumulative and monthly displacement shows that the slide mass deformed rather gradually from 2016 to 2017, but greatly accelerated in 2015 (Fig. 8b). The average velocity for monitoring points follows the same pattern as the displacement, decreasing from the right marginal part KD2-1 to the left marginal part KD2-3. The maximum average velocity is 3.6 cm/day at monitoring point A-1, while the minimum is 0.008 cm/day at monitoring point C-1 (Fig. 9).

Reservoir Water Level

KD2-1 slide mass indicates steadily continuous increased displacement at monitoring point A-1.

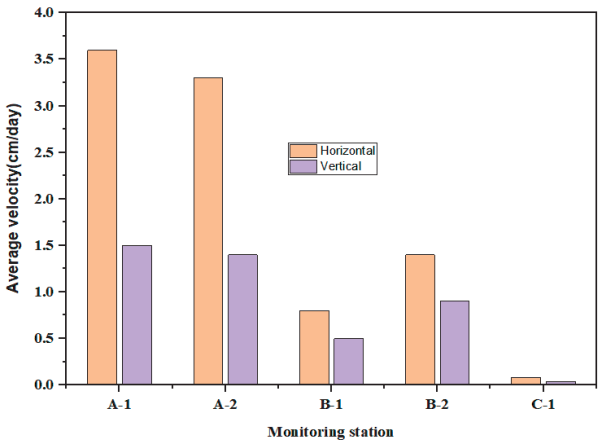

Fig. 9. Average velocities at 5 GPS monitoring points.

The annual velocity difference between high and low activities is 2.4 cm/day to 0.04 cm/day for horizontal velocity and 1.09 cm/day to 0.03 cm/day for vertical velocity. The maximum velocity observed when the reservoir level variation rate is greater than 0.5 m/day. The slide mass moved with an average speed of 0.42 cm/month in 2015 and 0.34 cm/month in 2016, respectively. Generally, an acceleration phase of displacement initiate in December and lasted until late March and then a persistent continuous displacement of low velocity began till the next phase (Fig. 10). Similar displacement acceleration phases are observed for remaining monitoring stations. So, deformation behavior is clearly synchronized with reservoir level changes. This deformation behavior can not be only related with reservoir level, some other factors such as rainfall can play an important role. In order to know the causes of velocity acceleration phases, the rainfall data is also analyzed.

Water progressively penetrates from the slope surface into the interior of the landslide body as the reservoir level rises, resulting in a large seepage force with the direction pointing inside the slide that grows gradually, which is good to the landslide's stability. The seepage field of the landslide body would remain relatively constant when the reservoir water level raised to a stable water level for a period of time, and the direction of seepage force in this stage would move to the outside of the slide. During declining reservoir level, the decline of the groundwater level generally tends to lag behind the reservoir water, leading to high seepage pressure and dynamic water pressure with directions pointing to the outside of the slide, which is detrimental to the landslide's stability.

Rainfall

The precipitation monitoring data from December 2104 to July 2016 is analyzed to develop a potential relationship between precipitation and slope velocity. Precipitation has the same temporal trend as reservoir

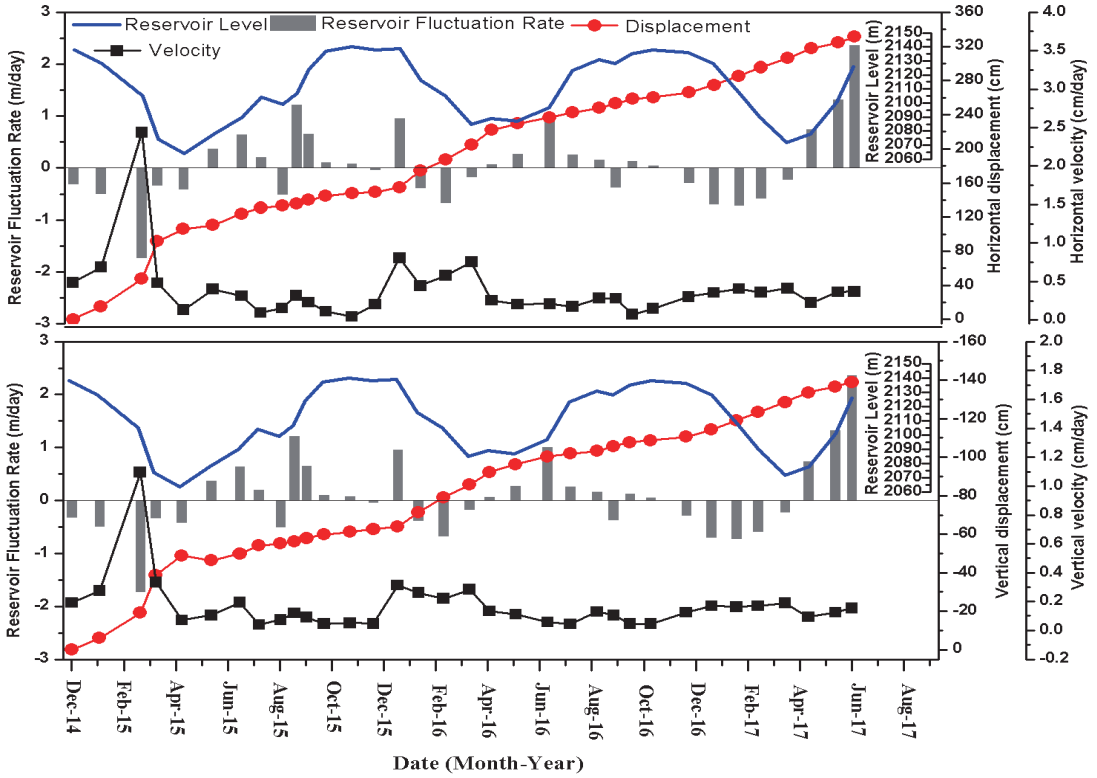

Fig. 10. Temporal relationship between reservoir level and displacement.

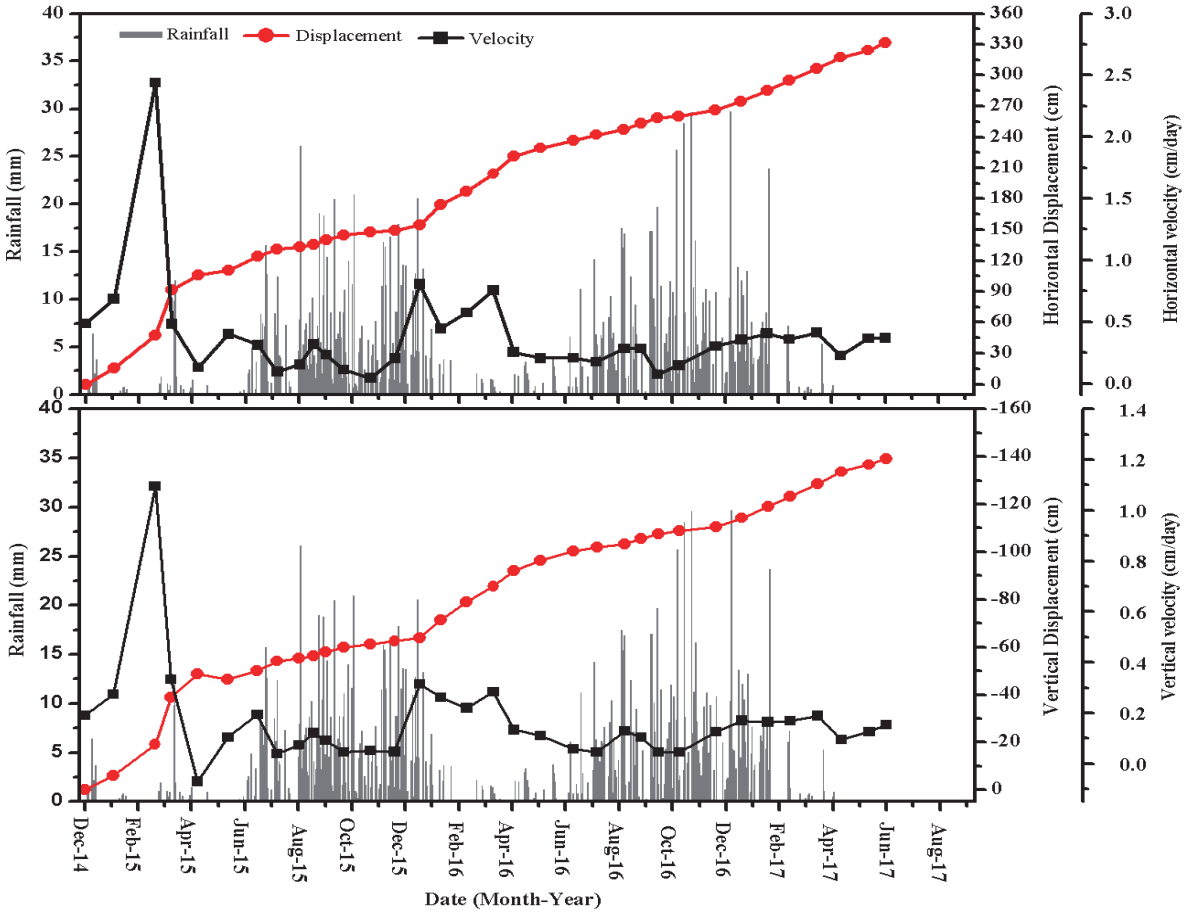

Fig. 11. Variation of slope velocity and precipitation.

level (decreases first and increases later in the year). The slope movement trend shows no clear correlation to precipitation (Fig. 11). The displacement velocity accelerated between December and March, while the heavy precipitation did not start before June. The asynchronous peaking behavior of rainfall and displacement velocity occured simultaneously. This indicates that precipitation is not the decisive trigger for the slope acceleration phase. After a detailed examination of GPS monitoring data, it is clear that the slide mass displacement curves typically show a phase of acceleration that only partly relates to the increased

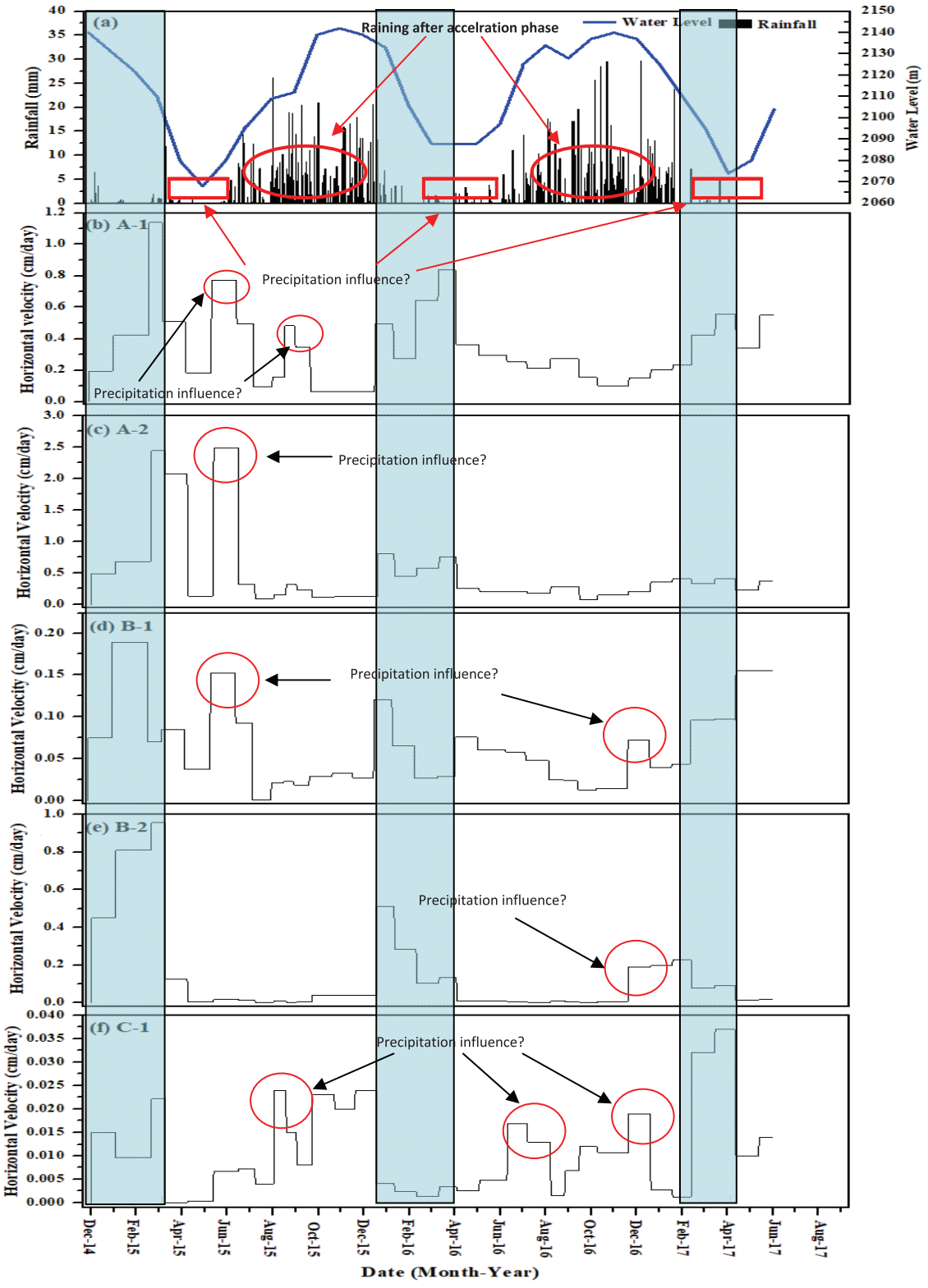

Fig. 12. Hydrological factors (Reservoir level and Precipitation) and variation in horizontal velocities.

precipitation during heavy rainfall. Precipitation considerably increases infiltration rate into the interior of the landslide body through the existing cracks, which causes saturation and results in a high pore-water pressure in the slip mass, enhancing the slide's downslide strength and deformation of the slide mass. Considering rain-water directly seep into slide mass, both pore water pressure and seepage outflow would be increased during the heavy rainy season and low reservoir period, so an additional mobilizing influence of rainfall during the low reservoir level is possible (bounded by red eclipse in Fig. 12).

Summary and Conclusions

The fundamental control on deformation of a partially submerged landslide is largely associated with the changes that occurred due to the reservoir level variation and precipitation. This study takes Kadui-2 landslide as a case study to examine the stability and deformation response under the influence of reservoir level and precipitation for a complete hydrological cycle. In-depth field investigations, drilling operation, surface deformation and hydrological monitoring were employed to study the factors that contributing to landslide. In order to understand the stability mechanism and seep lines characteristics, a two-dimensional finite element model was set up using SEEP/W and SLOPE/W modules of Geo-studio. High deformation rate and low stability occurred during reservoir-drawdown periods and rainy season. Based on the simulation results and monitored data, the following conclusions were reached.

- The Kadui-2 landslide is an active and planar soil mass slide. Based on the morphological distribution and monitoring system, the sliding mass comprises two active blocks, KD2-1, KD2-2, and a relatively stable block KD2-3.
- Analysis of displacement time series curves is characterized by rapid movements over a short period followed by a low and consistent displacement over a long period, which appears to follow a seasonal cycle correlating with reservoir level and rainfall. Seasonal rapid movements are synchronized with low reservoir level and high precipitation, giving rise to maximum speed 2.4 cm/day when the reservoir declining rate is 0.5 m/day. The pattern of displacement is dominantly controlled by the fluctuation of reservoir level only.
- Displacement curves of monitoring points on different location are inconsistent. This piece of evidence shows that the landslide deforms partly rather entirely.
- Simulation results reveal that the saturation zone lies below the maximum reservoir level (2140 m), seep lines and landslide stability lag behind the reservoir level. During the reservoir-filling, seep lines constrained to a large saturation zone and vice versa. The contributing factor for landslide stability is the reservoir filling-drawdown operation rather than precipitation. Without considering the rainfall, the stability coefficient is smaller by 1% only.
- The slide surface show significant creep influences, considering the long term strength, the landslide stability decreases gradually from less -stable state to worse-stable state.
- The right marginal part KD2-1 shows comparatively high deformation grade and large deformation occurred at the froeside of entire slide mass, so urgent necessary mitigation for prevention and control of the landslide are required. The findings of this study are useful for understanding the dynamic process of Qiaoqi reservoir landslides, effective remedial measures and as a reference for other landslides.

Acknowledgment

The authors are grateful to the National Key Research and Development Program (2018YFC1505401) for providing financially support for this study.

Conflicts of Interest

The authors declare no conflict of interest

References

1. HAN B., TONG B., YAN J., YIN C., CHEN L., LI D. The monitoring-based analysis on deformation-controlling factors and slope stability of reservoir landslide: Hongyanzi landslide in the southwest of China. Geofluids. 1, **2018**.
2. JIAN W., WANG Z., YIN K. Mechanism of the Anlesi landslide in the Three Gorges reservoir, China. Engineering Geology. **108**, 86, **2014**.
3. TANG H., LI C., HU X., WANG L., CRISS R., SU A., WU Y., XIONG C. Deformation response of the Huangtupo landslide to rainfall and the changing levels of the Three Gorges reservoir. Bulletin of Engineering Geology and the Environment. **74**, 933, **2015**
4. GARIANO S.L., BRUNETTI M.T., IOVINE G., MELILLO M., PERUCCACCI S., TERRANOVA O., VENNARI C., GUZZETTI F. Calibration and validation of rainfall thresholds for shallow landslide forecasting in Sicily, southern Italy. Geomorphology. **228**, 653, **2015**.
5. IGWE O., MODE W., NNEBEDUM O., OKONKWO I., OHA I. The analysis of rainfall-induced slope failures at Iva Valley area of Enugu State, Nigeria. Environmental Earth Sciences. **71**, 2465, **2014**.
6. LEPORE C., KAMAL S.A., SHANAHAN P., BRAS R.L. Rainfall-induced landslide susceptibility zonation of Puerto Rico. Environmental Earth Sciences. **66**, 1667, **2012**.
7. XIAO S., HU Z., LU S., MING C., CHEN D. Classification of reservoir-triggered landsldies in Three Gorges Reservoir area. Journal of Yangtze River Scientific Research Institute. **30**, 39-44, **2013**.

8. PENG R., HOU Y., ZHAN L., YAO Y. Back-analyses of landfill instability induced by high water level: Case study of shenzhen landfill. International Journal of Environmental. Research Public Health. **13**, 126, **2016**.
9. YIN Y.P., HUANG B., CHEN X., LIU G., WANG S. Numericalanalysisonwavegeneratedby the Qianjiangping landslide in Three Gorges Reservoir, China. Landslides. **12**, 355, **2015**.
10. WOLTER A., STEAD D., WARD B.C., CLAGUE J.J., GHIROTTI M. Engineering geomorphological characterisation of the Vajont slide, Italy, and a new interpretation of the chronology and evolution of the landslide. Landslides. **13** (5), 1067, **2016**.
11. SONG K., WANG F.W., YI Q.L., LU S.Q. Landslide deformation behavior influenced by water level fluctuations of the Three Gorges Reservoir (China). Engineering Geology. **247**, 58, **2018**.
12. GU D.M., HUANG D., YANG W.D., ZHU J.L., FU G.Y. Understanding the triggering mechanism and possible kinematic evolution of a reactivated landslide in the three Gorges Reservoir. Landslides, **14**, 2073, **2017**.
13. UDVARDI B., KOVÁCS I.J., SZABÓ C., FALUS G., ÚJVÁRI G., BESNYI A., BERTALAN É. Origin and weathering of landslide material in a loess area: a geochemical study of the Kulcs landslide, Hungary. Environmental Earth Sciences **75** (19), 1299, **2016**.
14. TOMÁS R., LI Z., LOPEZ-SANCHEZ JM., LIU P., Singleton A. Using wavelet tools to analyse seasonal variations from InSAR time-series data: a case study of the Huangtupo landslide. Landslides. **13** (3), 437, **2016**.
15. LI C., TANG H.M., HAN D.W., ZOU Z.X. Exploration of the creep properties of undisturbed shear zone soil of the Huangtupo landslide. Bulletin of Engineering Geology and Environment. **78** (2),1237, **2019**.
16. JOHANSSAN J.M.A. Impact of Water-Level Variations on Slope Stability. PhD thesis, Lulea University of Technology, Sweden. **2014**.
17. ACHARYA K. BHANDARY N. DAHAL R. YATABE R. Numerical analysis on influence of principal parameters of topography on hillslope instability in a small catchment. Environmental Earth Sciences. **73**, 5643, **2015**.
18. TAKE W., BEDDOE R., DAVOODI-BILESAVAR R., PHILLIPS R. Effect of antecedent groundwater conditions on the triggering of static liquefaction landslides. Landslides. **12**, 469, **2015**.
19. PENDER M., ORENSE R., WOTHERSPOON L., STORIE L. Effect of permeability on the cyclic generation and dissipation of pore pressures in saturated gravel layers. Geotechnique. **66**, 313, **2016**.
20. CAO C., WANG Q., CHEN J., RUAN Y., ZHENG, L., SONG S. NIU C. Landslide susceptibility mapping in vertical distribution law of precipitation area: Case of the Xulong hydropower station reservoir, Southwestern China. Water. **8**, 248, **2016**.
21. XU Q., LIU H.X., RAN J.X., LI W.H., SUN X. Field monitoring of groundwater responses to heavy rainfalls and the early warning of the Kualiangzi landslide in Sichuan Basin, southwestern China. Landslides. **13**, 1555, **2016**.
22. WANG X.G., YIN Y.P., WANG J.D., LIAN B.Q., QIU H.J., GU T.F. A nonstationary parameter model for the sandstone creep tests. Landslides. **15**, 1377, **2018**.
23. TANG H.M, LI C.D, HU X.L, WANG L.Q, ROBERT C, SU A.J, WU Y.P, XIONG C.R. Deformation response of the Huangtupo landslide to rainfall and the changing levels of the Three Gorges Reservoir. Bulletin of Engineering Geology and Environment. **74**, 933, **2015**.
24. IQBAL J., TU X., XU L. Landslide Hazards in the Reservoir Areas: A Case Study of Xiangjiaba Reservoir, Southwest China. Natural Hazards Review. **18**, 1, **2017**.
25. ALMEIDA S., HOLCOMBE E.A., PIANOSI F., WAGENER T. Dealing with deep uncertainties in landslide modelling for disaster risk reduction under climate change. Natural Hazards Earth System Science. **17**, 225, **2017**.
26. YIN Y., HUANG B., WANG W. Journal of rock mechanics and geotechnical engineering reservoir-induced landslides and risk control in Three Gorges Project on Yangtze River, China Journal of Rock Mechanics and Geotechnical Engineering. **8**, 577, **2016**.
27. WANG J., XIANG W., LU N. Landsliding triggered by reservoir operation: a general conceptual model with a case study at Three Gorges Reservoir. Acta Geotech. **9**, 771, **2014**.
28. HOU T.S., XU G.L., SHEN Y.J., WU Z.Z., ZHANG N.N., WANG R. Formation mechanism and stability analysis of the Houba expansive soil landslide. Engineering Geology. **161**, 34, **2013**.
29. QI S.C., SAI K. Influence of swelling behavior on the stability of an infinite unsaturated expansive soil slope. Computer and Geotechnics. **76**, 154, **2016**.
30. TANG L., CONG S., GENG L., LING X., GAN F. The effect of freeze-thaw cycling on the mechanical properties of expansive soils. Cold Region Science and Technology. **145**, 197, **2018**.
31. ALONSO E.E., GENS A., DELAHAYE C.H. Influence of rainfall on the deformation and stability of a slope in over consolidated clays: a case study. Journal of Hydrogeology. **11**, 174, **2003**.
32. PERUCCACCI S., BRUNETTI M.T., LUCIANI S., VENNARI C., GUZZETTI F. Lithological and seasonal control on rainfall thresholds for the possible initiation of landslides in Central Italy. Geomorphology. **139**, 79, **2012**.
33. GUZZETTI F., STARK C.P., SALVATI P. Evaluation of flood and landslide risk to the population of Italy. Environmental Management. **36**, 15, **2016**.
34. IADANZA C., TRIGILA A., NAPOLITANO F. Identification and characterization of rainfall events responsible for triggering of debris flows and shallow landslides. Journal of Hydrology. **541**, 230, **2016**.
35. YAO W.M., LI C.D., ZUO Q.J., ZHAN H.B., ROBERT, E. Spatiotemporal deformation characteristics and triggering factors of Baijiabao landslide in three Gorges Reservoir region, China. Geomorphology. **343**, 34, **2019**.
36. VALLET A., CHARLIER J.B., FABBRI O., BERTRAND C., CARRY N., MUDRY J. Functioning and precipitation-displacement modelling of rainfall-induced deep-seated landslides subject to creep deformation. Landslides. **13**, 653, **2016**.
37. WIECZOREK G.F., GEIST E.L., MOTYKA R.J., MOTYKA R.J., JAKOB M. Hazard assessment of the tidal inlet landslide and potential subsequent tsunami, Glacier Bay National Park, Alaska. Landslides. **4**, 205, **2007**.
38. HARILAL G.T., MADHU D., RAMESH M.V., PULLARKATT D. Towards establishing rainfall thresholds for a real-time landslide early warning system in Sikkim, India. Landslides. **16** (12), 2395, **2019**.
39. PASTOR M., HADDAD B., SORBINO G., CUOMO S., DREMPETIC V. A depth-integrated, coupled SPH model for flow-like landslides and related phenomena. International Journal for Numerical and Analytical Methods in Geomechanics. **33**, 143, **2009**.

40. CHAE B.G., PARK H.J., CATANI F., SIMONI A., BERTI M. Landslide prediction, monitoring and early warning: a concise review of state-of-the-art. Geosciences Journal, **21**, 1033, **2017**.
41. LIU X.R., JIN M.H., LI D.J., ZHANG L. Strength deterioration of a Shaly sandstone under dry-wet cycles: a case study from the Three Gorges Reservoir in China. Bulletin of Engineering Geology and the Environment. **77** (4), 1607–1621, **2018**.
42. AKGUN A., KINCA C., PRADHAN B. Application of remote sensing data and GIS for landslide risk assessment as an environmental threat to Izmir city (west Turkey). Environmental Monitoring and Assessment. **184**, 5453, **2011**.
43. PASCULLI A., SCIARRA N., ESPOSITO L., ESPOSITO AW Effects of wetting and drying cycles on mechanical properties of pyroclastic soils. Catena. **156**, 113, **2017**.
44. COOK K.L., ROYDEN L.H., BURCHFIEL B.C., LEE Y.H., TAN X. Constraints on Cenozoic tectonics in the southwestern Longmen Shan from low-temperature thermo chronology. Lithosphere. **5**, 393, **2013**.
45. ZHANG Y.Q., DONG S.W., HOU C.T., SHI J.S., WU Z.H., LI H.L., SUN P., LIU G., LI J. Seismogenic structure of the April 20, 2013, Lushan Ms 7 earthquake in Sichuan. Acta Geologica Sinica. **87**, 633, **2013**.
46. HE K., LI Y., MA G., HU X., LIU B., MA Z., XU Z. Failure mode analysis of post-seismic rockfall in shattered mountains exemplified by detailed investigation and numerical modeling. Landslide, **2020**, (accepted).
47. TANG H., LI C., HU X. Evolution characteristics of the Huangtupo landslide based on in situ tunneling and monitoring. Landslides. **12**, 511, **2015**.
48. UDVARDI B, KOVÁCS IJ, SZABÓ C, FALUS G, ÚJVÁRI G, BESNYI A, BERTALAN É. Origin and weathering of landslide material in a loess area: a geochemical study of the Kulcs landslide, Hungary. Environmental Earth Sciences **75** (19), 1299, **2016**.